Research Article | Vol. 29, No. 19 / 13 Sep 2021 / Optics Express 30104
Optics EXPRESS

Single-layer graphene optical modulator based on arrayed hybrid plasmonic nanowires

ZHIKAI LI,[1,2] JIYUAN HUANG,[1,2] ZHUOHANG ZHAO,[1] YULIN WANG,[1,*] CHENGPING HUANG,[1] AND YONG ZHANG[1]

[1]Department of Physics, Nanjing Tech University, Nanjing 210009, China
[2]contributed equally to this work
[*]yulinwang@njtech.edu.cn

Abstract: Surface plasmon-polaritons (SPPs)-based waveguides, especially hybrid plasmonic nanowires, which have attracted extensive interests due to easy fabrication, high transmittance, subwavelength mode confinement and long propagation distance, are appropriate platforms for enhancing the interaction with graphene. Considering that graphene is a two-dimensional (2D) material with surface conductivity, it is important to enhance the in-plane electrical components parallel to graphene. Here, we propose a tunable graphene optical modulator based on arrayed hybrid plasmonic nanowires, utilizing strong subwavelength confinement of gap-surface plasmonic modes (GSPMs) and near-field coupling in the periodic metasurface structure to enhance effective light-matter interactions. The modulator has a typical modulation depth (MD) of 4.7 dB/μm, insertion loss (IL) of 0.045 dB/μm, and a broadband response. The modulation performance can be further optimized, achieving MD of 16.7 dB/μm and IL of 0.17 dB/μm. Moreover, with the optimized modulator, the 3 dB bandwidth can reach 200 GHz. The energy consumption of modulator is about 0.86 *fJ/bit*. Our design exhibits fascinating modulation performance, fabrication compatibility and integration potential. It may inspire the schematic designs of graphene-based plasmonic modulator and pave a way to the application of 2D materials-involved optoelectronic devices.

1. Introduction

Graphene as a two-dimensional (2D) atomically thin carbon nanomaterial, possesses unique photoelectric properties, good thermal conductivity, stability, and excellent carrier mobility, with tremendous application potentials in designing optoelectronic devices [1–4]. It is an excellent electro-optical material that can enable next-generation photonic modulators with the desired features, since it has exceptional properties such as large carrier mobility, wide response range and electrically tunable optical absorption. In 2011, Liu et al. first introduced graphene into modulators by placing single- or double-layer graphene on a silicon waveguide to modulate the dielectric waveguide modes [5,6]. Subsequently, many other graphene-embedded and multi-layer graphene silicon modulators have been proposed to enhance the light-matter interaction [7–10]. In addition, graphene modulators can be used to improve the performance of all-fiber modulator and greatly reduce device losses [11]. However, the maximal electric field of guided modes in silicon waveguide is confined in the center, leading to small overlap between the optical mode and graphene sheet. It makes the graphene-on-silicon modulator has large footprint and high energy consumption, limiting the improvement of modulation performance.

Surface plasmon-polaritons (SPPs) are characterized of subwavelength mode confinement beyond the diffraction limit. Especially, the graphene plasmons own advantageous optical properties of extreme field confinement and low losses, and attract extensive research interests [12–15]. Therefore, SPPs are suitable candidates for enhancing the interaction between light and graphene [16–20]. With the development of various plasmonic modulators, the modulation depths (MD) of single-layer graphene modulators have reached to 0.03-12 dB/μm [21–31].

#434916 https://doi.org/10.1364/OE.434916
Journal © 2021 Received 7 Jul 2021; revised 22 Aug 2021; accepted 23 Aug 2021; published 1 Sep 2021

Optics EXPRESS

Especially, hybrid plasmonic nanowire attracts extensive research interests attributed to easy fabrication, high transmittance, subwavelength mode confinement and long propagation distance, with various applications for surface enhanced Raman scattering (SERS), remote excitation of fluorescence, signal routing, biomolecular detections and laser [32–34]. Thus, graphene optical modulator based on hybrid plasmonic nanowires can be an excellent alternative. In many theoretical studies, MD has been over-estimated by considering graphene as an isotropic three-dimensional (3D) material with effective thickness and permittivity [35–38]. Regarding that graphene is a 2D material with surface conductivity, another key to promote modulation efficiency is increasing the in-plane electric field components parallel to graphene, except for increasing the mode overlap with graphene. Thanks to mode coupling in the periodic metasurface structure, the optical modes can be confined well below the diffraction limit and the in-plane electric field components are strengthened. Therefore, graphene modulator based on periodically arrayed hybrid plasmonic nanowires is a potential scheme for modulator design, providing a possible solution to improve the modulation efficiency.

In this work, a tunable graphene optical modulator based on arrayed plasmonic nanowires is proposed, as shown in Fig. 1. The modulator is constructed by arrayed silver nanowires atop a subwavelength-thin dielectric spacer and optically thick silver substrate, a configuration that supports gap-surface plasmonic modes (GSPMs). The diameter of the silver nanowire is defined as d, the period is p, and the dielectric layer thickness is h (see the cross-section in Fig. 1). The graphene covers the upper surface of the dielectric spacer, where the electric field of GSPM is significantly enhanced by the strong field confinement, so the interaction between light and graphene can be greatly improved. The graphene optical modulator is composed of well-arranged Ag nanowire arrays, so the electromagnetic modes supported in GSPMs can be investigated by analyzing the eigenmodes of the nanowire waveguides with periodic boundary conditions. It is known that conventional SPP mode has its main electric field component oriented along the normal direction of the metal surface, which is harmful to effective interaction with graphene. Thanks to the strong confinement of GSPM and coupling of the two adjacent silver nanowires, the electric field intensity is tightly confined at the graphene plane. Moreover, the parallel field components will increase, which match the direction of the graphene plane. In this perspective, it is expected to improve the SPP-graphene interaction.

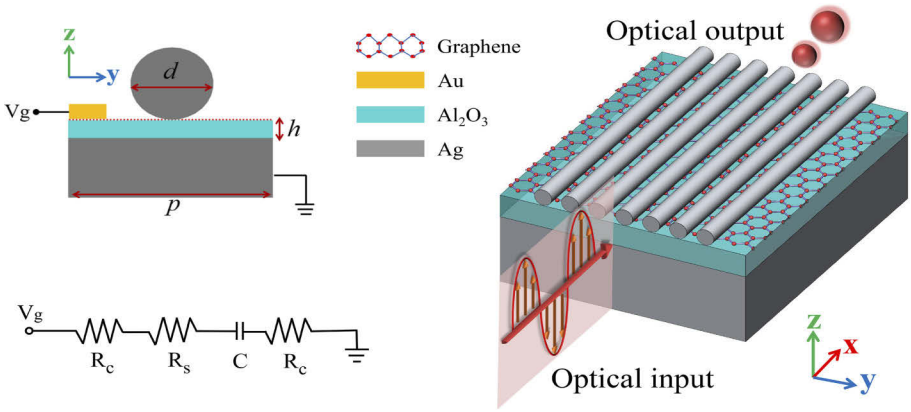

Fig. 1. Schematics of the graphene optical modulator based on arrayed hybrid plasmonic nanowires. The cross-section of unit cell of the modulator in the y-z plane is shown in the top-left inset. The equivalent electric circuit of this modulator is depicted in the bottom-left inset.

Optics EXPRESS

2. Eigenmode analysis of arrayed hybrid plasmonic nanowires

Full-field electromagnetic wave simulations are performed using the finite element solver (COMSOL Multiphysics) to study the eigenmodes of the Ag nanowire hybrid plasmonic waveguides without graphene. The working wavelength is set as 1310 nm. A 2D eigenmode analysis of the arrayed hybrid plasmonic nanowires (as shown in the inset of Fig. 1) is performed in the unit cell with periodic boundary conditions along the y-axis, where the unit period p is 100 nm. The diameter d of Ag nanowire is 60 nm, the permittivity of silver is $\varepsilon_m = -90.305 + 2.1144i$, according to the experimental data (Johnson and Christy 1972) [39]. The dielectric spacer is filled by Al_2O_3 with refractive index $n_{AlO} = 1.75$, and the thickness $h = 10$ nm. According to the mode analysis, there are two eigenmodes strongly confined in the spacer gap (see the inset of Fig. 2(a)), which can be excited by z-polarized wave. Unlike free SPP on a flat metal surface, the electric fields of these two modes at the position of upper surface of dielectric layer have an obvious enhancement. Especially, the E_y component is strengthened, which matches the conductivity of the graphene plane. Therefore, more components participate in effective interaction, improving the modulation depth. To deeply understand the feature of the two modes, we study the real and imaginary parts of the effective mode indices (EMI) as functions of the unit period p, indicated in Fig. 2(a).

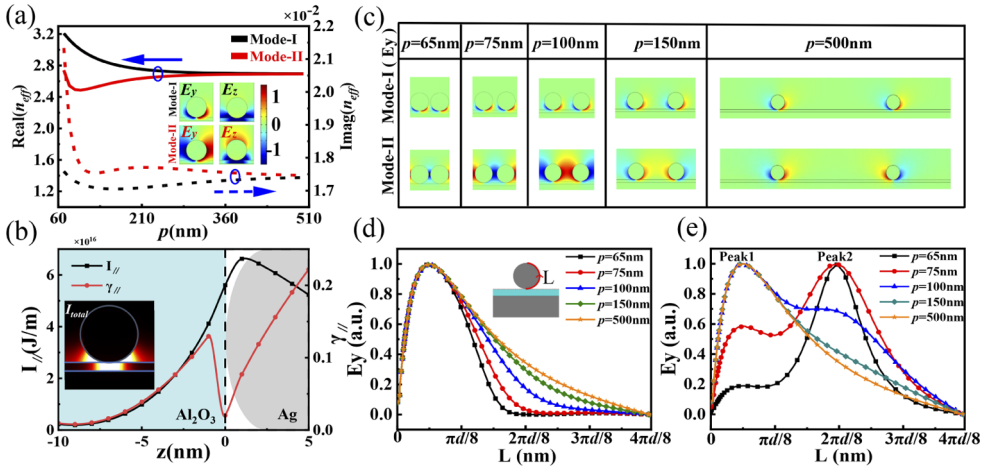

Fig. 2. (a) The real and imaginary parts of EMI with respect to the period p. The insets are the E_y and E_z components of Mode-I and Mode-II. The working wavelength is set as 1310 nm. (b) The distribution for intensity of in-plane components $I_{||}$ and the in-plane ratio $\gamma_{||}$ with different height z. (c) The distributions of E_y component for Mode-I and Mode-II with different periods. (d), (e) the electric field distributions along the nanowire surface for Mode-I and Mode-II.

Based on the electric field distributions of the two modes, one can see that the E_y and E_z components of two adjacent nanowires are in-phase for Mode-I and anti-phase for Mode-II. So, Mode-I is symmetric mode, while Mode-II is anti-symmetric mode. When the period is equal to 500 nm, the two modes are almost degenerate because of a weak coupling between adjacent plasmonic nanowire waveguides. With the period decreasing, the near-field coupling between adjacent plasmonic nanowire waveguides gets stronger, as shown in Fig. 2(c). For symmetric Mode-I, the electric field components in the air gap between two nanowires are anti-phase, and will repel each other. When p<300 nm, the coupling of plasmonic nanowires grows fast. According to the electric field distributions along the nanowire exterior boundary as shown with the red arrow in the inset of Fig. 2(d), the equivalent wavelength of E_y reduces as the period decreases, so the real part increases. For anti-symmetric Mode-II, the field distributions of E_y

Optics EXPRESS

component of two adjacent plasmonic nanowires are mirror symmetric, and will be strongly coupled together for small period. As shown in Fig. 2(e), when p is smaller than 100 nm, the peak of E_y component appears at Peak2. With the increase of period p, the distribution peak gradually shifts from Peak2 to Peak1, and the confinement gets worse. The critical coupling takes place when p = 100 nm, thus, the real part of Mode-II decreases at first and then increases. In general, the imaginary parts of two modes increase due to the stronger Ohmic loss of metal with stronger mode confinement. While, it changes little because of weak coupling when p>100 nm. According to the imaginary part, the propagation length is about 6.2 μm, which is enough for subwavelength integrated modulator in this work. Particularly, the anti-symmetric Mode-II cannot be excited by a uniform z-polarized electromagnetic wave, so it is difficult to use Mode-II in experiment. Considering a possible practical excitation, the in-phase Mode-I is more accessible. Therefore, we will mainly investigate Mode-I for the function of a plasmonic modulator. To investigate the physical mechanism of interaction between matter and the localized electric field of Mode-I at the position of upper surface of dielectric layer (the plane of graphene), the in-plane components ratio $\gamma_{\parallel}$ [40] and the localized field confinement ratio η_c of the eigenmode are studied. Two ratios are defined as:

$$\gamma_{\parallel} = \frac{I_{\parallel}}{I_{total}} = \frac{\iint_S |E_{\parallel}|^2 \, dS/S}{\iint_S |E_{total}|^2 \, dS/S} \tag{1}$$

$$\eta_c = \frac{\iiint_{V_c} |E_{total}|^2 \, dV}{\iiint_{V_{total}} |E_{total}|^2 \, dV} \tag{2}$$

Here, $E_{\parallel}$ is the in-plane components, including E_x and E_y. S represents the area of upper surface of dielectric layer. The field confinement ratio η_c is the ratio of the mode field in the volume V_c near the graphene to the total mode field. The volume is $V_c = h_c * S$. For calculation, h_c is set as 1 nm considering the thickness of graphene. According to the inset of Fig. 2(b), as approaching to the upper surface, the electric field strengthens, and the field confinement ratio near graphene is η_c = 13.8%. Simultaneously, the in-plane components increase, which is beneficial for the SPP-graphene iteration.

3. Modulation performance based on 2D mode analysis

Next, a plasmonic modulator covered with a thin layer of graphene is considered. In simulation, we use an anisotropic graphene model with in-plane conductivity. Graphene's complex conductivity depends on the radian frequency ω, carrier relaxation time τ, temperature T, and Fermi level E_f. The conductivity of graphene can be described by Kubo formula [41,42]. The modulator's performance is determined by the photoelectric absorption mechanism of graphene, caused by intraband and interband transitions. The simplified intraband conductivity can be described as:

$$\sigma_{intra}(\omega) = \frac{je^2 E_f}{\pi\hbar^2 \left(\omega + j\tau^{-1}\right)} \tag{3}$$

and the interband conductivity can be expressed as:

$$\sigma_{inter}(\omega) = \frac{je^2}{4\pi\hbar} ln\left(\frac{2\left|E_f\right| - \left(\omega + j\tau^{-1}\right)\hbar}{2\left|E_f\right| + \left(\omega + j\tau^{-1}\right)\hbar}\right) \tag{4}$$

$$\sigma_{total} = \sigma_{intra}(\omega) + \sigma_{inter}(\omega) \tag{5}$$

where σ_{total} is the conductivity of monolayer graphene, e is the charge of an electron, $\hbar = h/2\pi$ is the Planck constant. The carrier relaxation time τ depends on the carrier mobility μ of graphene

Optics EXPRESS

($\tau = \mu E_f / eV_f^2$), where $\mu = 0.3m^2/(V \cdot s)$ and $V_f = 1 \times 10^6 m/s$ is the Fermi velocity in graphene. Figure 3(a) shows the real and imaginary parts of graphene's conductivity. In addition, we can get the Fermi level according to the driving voltage V_g with formula as:

$$E_f = \hbar V_f \sqrt{\pi \epsilon_0 \epsilon_d / (e d_g) \mid V_g - V_{Dirac} \mid} \tag{6}$$

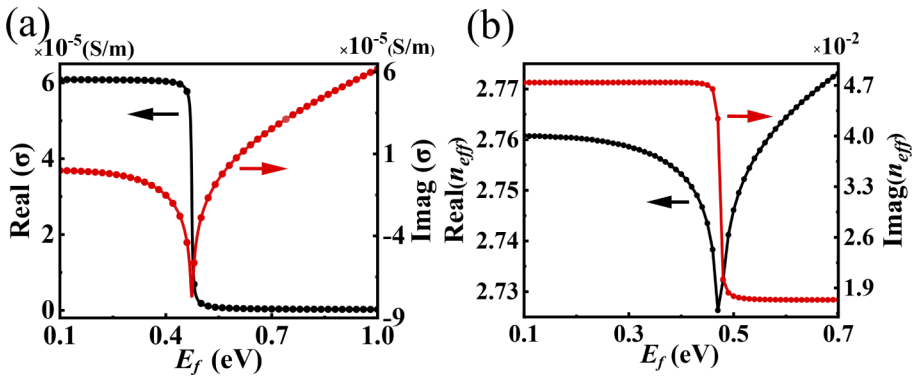

Fig. 3. (a) Real and imaginary parts of surface conductivity of graphene. (b) Real and imaginary part of EMI with Fermi level varying.

Among them, d_g, ϵ_d represent the thickness and the dielectric constant of the Al_2O_3 insulator. $\mid V_g - V_{Dirac} \mid$ defines external gate voltage, V_{Dirac} stands for the offset voltage caused by natural doping.

Based on the calculation of in-plane conductivity, the modulation performance can be simulated. The MD can be estimated by the change of the eigenmodes of plasmonic nanowire waveguide with graphene as a function of the Fermi level E_f. At low gate voltage, the Fermi level of graphene is lower than the threshold ($E_f < \hbar\omega/2 = 0.48eV$), the external photons will be absorbed, leading to interband transition. The eigenmode will have a large loss, corresponding to a large imaginary part of EMI, and this is so-called OFF-state ($E_f = 0.4eV$). At a high gate voltage, the Fermi level will exceed the transition threshold ($E_f > \hbar\omega/2$), the external photons can't be absorbed due to absorption saturation. The graphene is transparent and the absorption loss is low, corresponding to a small imaginary part, referred as ON-state ($E_f = 0.6eV$). Therefore, the MD can be estimated by the difference between two imaginary parts of ON/OFF states. Figure 3(b) exhibits the real and imaginary parts of EMI ($d = 60$ nm, $p = 200$ nm, $h = 10$ nm) with Fermi level changing, and the MD can be calculated as 1.25 dB/μm. MD can be calculated by the imaginary parts of EMI, as shown in formulas 7, 8:

$$\alpha = \frac{10 Im(n_{eff}) 4\pi}{\lambda_0 \ln 10} \tag{7}$$

$$MD = \alpha(OFF) - \alpha(ON) \tag{8}$$

According to the analysis of eigenmode distribution, the electric fields at the position of graphene have an obvious enhancement. Besides, E_x and E_y components are strengthened, which match the plane of the graphene's surface conductivity. Therefore, more components participate in effective interactions, improving the performance of modulator. Furthermore, the structural parameters of plasmonic nanowire modulator are optimized, illustrated in Fig. 4. As shown in the inset of Fig. 4(a), when the period is large, the difference in modulation performance is relatively small. The influence of period on MD is weak, while the diameters of nanowires have an obvious impact, depicted in Fig. 4(a). In the following study, the period is fixed as 100 nm, considering fabrication feasibility. Then, the modulation performances on the diameter d

Optics EXPRESS

and the dielectric layer thickness h have been studied, depicted in Fig. 4(b). The MD can be optimized when d and h decrease. Compared with diameter, the influence of the thickness is weaker. Finally, the plasmonic nanowire modulator has a MD of 4.56 dB/μm with structural parameter of d = 20 nm, h = 10 nm and p = 100 nm. Besides, the insertion loss (IL) and Q factor are calculated, in order to fully confirm the performance of graphene optical modulator. IL, the difference in propagation loss between with and without graphene, is relatively low with 0.045 dB/μm. Therefore, Q factor, as the ratio of MD to IL, is 101 and performs well. Compared with the currently reported single-layer graphene modulator [21–24], it has a significant improvement.

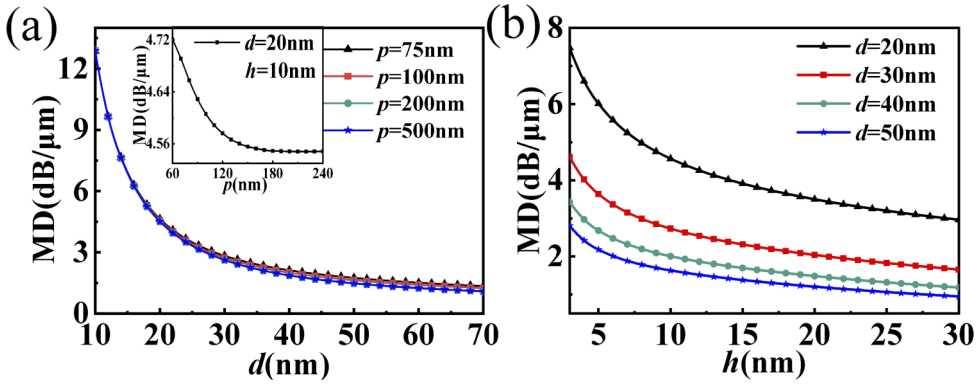

Fig. 4. (a) The MD varies with the diameter of nanowire d at several periods. The inset shows the dependence of MD on the period with d = 20 nm and h = 10 nm. (b) The MD varies with the thickness of the dielectric spacer h at several d values.

4. Modulation performance based on 3D propagation analysis

In order to verify the results of modulation performance based on 2D eigenmode analysis, a 3D propagation simulation model of Mode-I with a continuous period boundary is performed (as shown in Fig. 1). The MD can be directly calculated according to the transmission coefficient and propagation distance. We calculate the transmission coefficient of silver nanowire structure model with a propagating distance of 1 μm at different Fermi levels, described in Fig. 5(a). Through propagation mode analysis, the MD can be calculated according to the ratio of transmission coefficient of ON-state and OFF-state. A MD of 4.7 dB/μm is achieved, and the IL is 0.045 dB/μm, finally Q factor of 104 is obtained. These results are consistent well with those calculated by 2D eigenmode analysis, proving the accuracy of previous calculation. From the curve of transmission, the case of E_f<0.48eV corresponds to the state of "OFF", and E_f>0.48eV is "ON" state. The propagation mode field distributions of the ON-state and OFF-state are shown in the inset of Fig. 5(a). Furthermore, the broadband response of plasmonic nanowire optical modulator is calculated. As illustrated in Fig. 5(b), the black line represents the MD of 2D eigenmode analysis, and the red one represents 3D propagation mode analysis. The MD performance maintains well at the working wavelength from 800 nm to 1900 nm.

Moreover, the modulation performance can be further improved with the parameter of p = 50 nm, d = 10 nm and h = 5 nm. In this case, the MD is increased to 16.7 dB/μm and the IL is 0.17 dB/μm. The Q factor is maintained at a high level of 98, with a relatively broadband response. Figure 6(a) exhibits the modulation performances on the diameter d and the dielectric layer thickness h. It shows that d has a great influence on modulation performance, MD can even reach 59 dB/μm with d of 5 nm. Simultaneously, the real and imaginary parts of EMI (d = 10 nm, p = 50 nm, h = 5 nm) with Fermi level changing are shown in Fig. 6(b). Subsequently, the transmission coefficient of silver nanowire structure model with a propagating distance of 1 μm

Optics EXPRESS

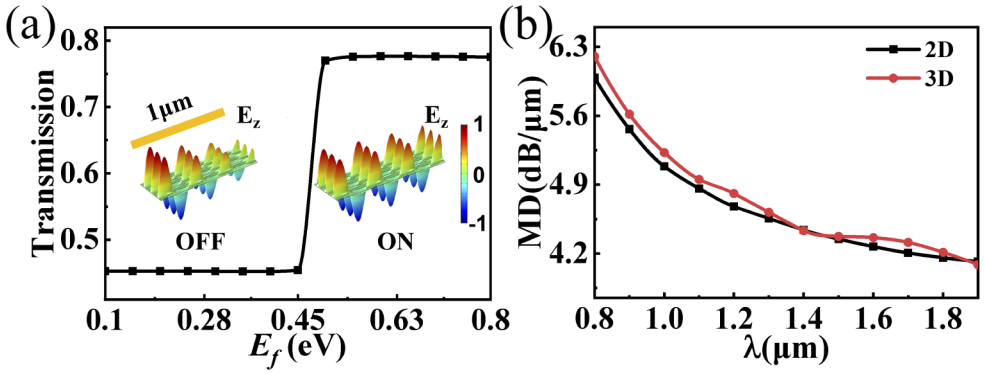

Fig. 5. (a) Transmission coefficient curve with respect to different E_f calculated by 3D propagation simulations, in which the electric field of E_z component for OFF-state (E_f = $0.4eV$) and ON-state (E_f = $0.6eV$) are depicted. (b) MD curves of broadband response (λ=800-1900nm), 2D eigenmode analysis (black) and 3D propagation mode analysis (red).

at different Fermi levels has been caculated, as described in Fig. 6(c). Besides, the broadband response can also be analyzed, as depicted in Fig. 6(d). The in-plane components ratio $\gamma_{\|}$ and the field confinement ratio η_c of the localized electric field of Mode-I near graphene are also studied, revealing the relationship between MD and the distribution of eigenmode without graphene (Fig. S1, Supplement 1).

The electrical parameters such as 3 dB modulation bandwidth f_{3dB} and energy consumption per bit E_{bit} [43,44] are important criteria for evaluating the electrical performance of modulators. The equivalent electric circuit of this modulator is depicted in the bottom-left of Fig. 1. In this model, the capacitor C is the parallel-plate capacitor formed by the structure of graphene-Al_2O_3-silver slab, and the capacitance can be evaluated with $C = \varepsilon_0\varepsilon_d S/d_g$. So the calculated capacitance is $1.59fF$. The energy consumption per bit E_{bit} is defined as :

$$E_{bit} = C\,(\Delta V)^2\,/4 \tag{9}$$

where ΔV is the switching voltage between ON-state and OFF-state, can be calculated according to Equation (6). So E_{bit} is $0.86fJ/bit$. By using a RC circuit model, the 3 dB modulation bandwidth of proposed modulator is calculated by the following formulas:

$$R_{total} = R_s \times \frac{W_g}{L} + \frac{R_c}{L} \tag{10}$$

$$f_{3dB} = \frac{1}{2\pi R_{total} C} \tag{11}$$

$W_g = 2\ \mu m$ is active-width of the graphene and $L = 1\ \mu m$ is the length of modulator. In calculation, the sheet resistance $R_s = 200\Omega/\square$, and the contact resistance $R_c = 100\Omega\mu m$[44]. The contact resistance of bottom silver layer can be neglected for small resistivity and large contact area. Thus, the 3 dB modulation bandwidth f_{3dB} is 200 GHz. Thanks to the strong confinement and enhanced in-plane components, the MD is greatly increases, and device integration is improved also. Therefore, 3 dB modulation bandwidth and energy consumption improve, providing a schematic design for subwavelength integrated modulator.

The data in Fig. 7 describe the trend of previous modulator's performances in MD and IL . Up to now, for single-layer graphene modulators, MD has changed from 0.03 to 12 dB/μm [10,21–31]. Our modulator achieves significant progress in MD and maintains a comparatively low IL, leading to a well Q factor. The modulation performance can be further improved with sodium-based [45]

Optics EXPRESS

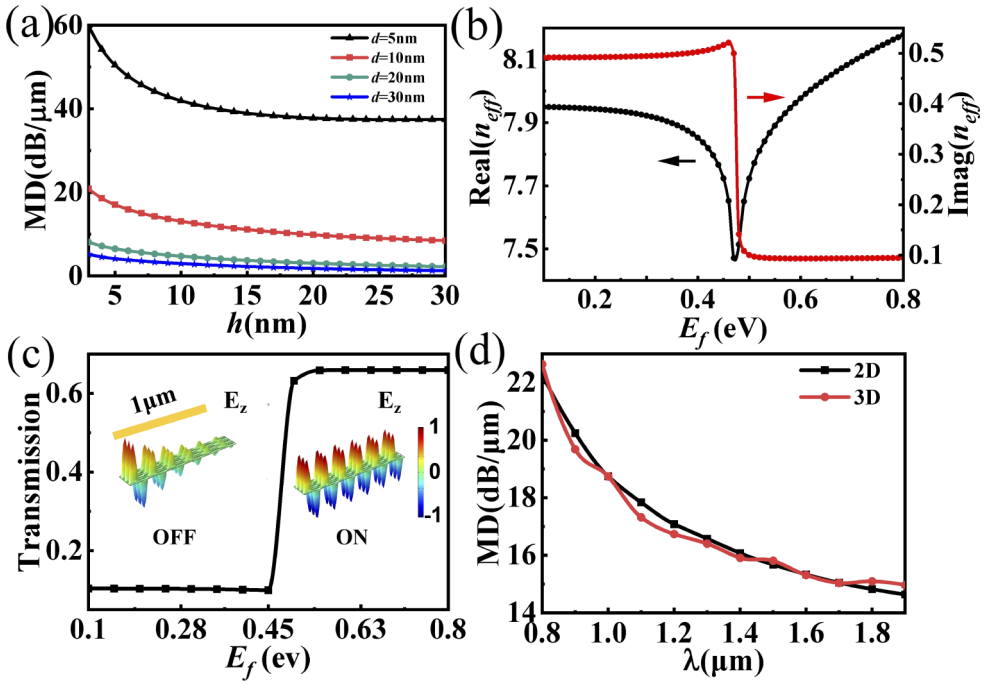

Fig. 6. (a) The MD varies with the thickness of the dielectric spacer h at several d values. (b) Real and imaginary part of EMI with Fermi level varying. (c) Transmission coefficient curve with respect to different E_f calculated by 3D propagation simulations, in which the electric field of E_z component for OFF-state (E_f = 0.4eV) and ON-state (E_f = 0.6eV) are depicted. (d) MD curves of broadband response (λ=800-1900nm), 2D eigenmode analysis (black) and 3D propagation mode analysis (red).

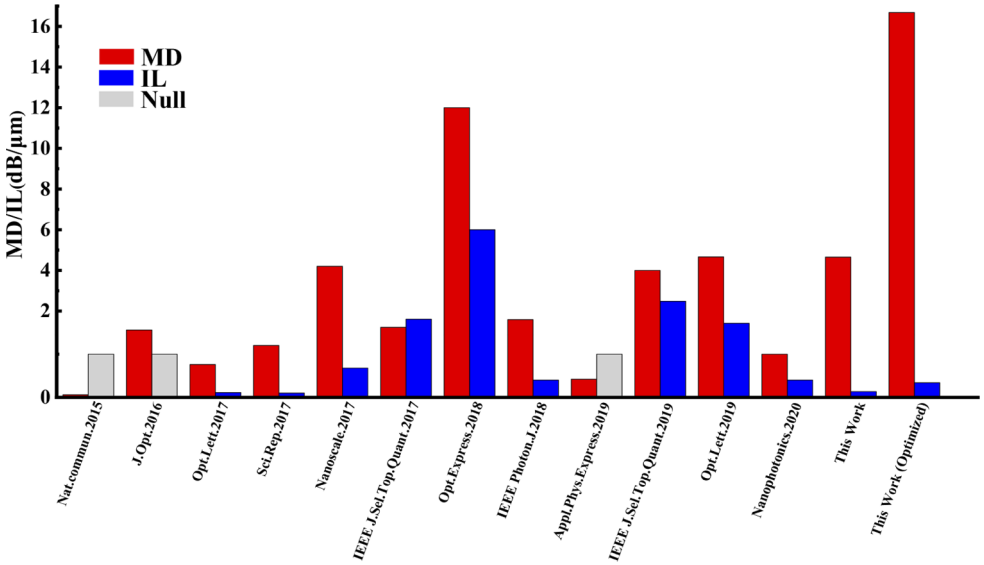

Fig. 7. Comparison between previous works and our work with MD and IL

Optics EXPRESS

plasmonic nanowire, which has a lower loss than noble metals (Fig. S2, Supporting material). This design scheme can improve the modulation performance and device integration, paving a way to solve the single-layer graphene optical modulator with hybrid plasmonic system.

5. Conclusion

In conclusion, we have proposed a tunable graphene optical modulator based on arrayed hybrid plasmonic nanowires. Thanks to the strong confinement of GSPM and the near-field coupling of the two adjacent silver nanowires, the electric field intensity is tightly confined in the subwavelength regime. The parallel field components increase, which match the direction of the graphene plane. Thus, it is supposed to further improve the SPP-graphene interaction. The plasmonic nanowire modulator has a MD of 4.7 dB/μm and IL is relatively low with 0.045 dB/μm. The Q factor is 104 and performs well with a broadband response. The MD performance can be further optimized, achieving MD of 16.7 dB/μm and IL of 0.17 dB/μm. By comparing our work with recent related work in detail, in terms of MD and IL, our single-layer graphene modulator has an obvious advantage. Moreover, with the optimized modulator, the 3 dB bandwidth can reach 200 GHz. The energy consumption of modulator is about $0.86fJ/bit$. Our design exhibits fascinating modulation performance, fabrication compatibility, high integration, low energy consumption and high modulation speed, which may inspire the schematic designs of graphene-based plasmonic modulators and pave a way to the applications of 2D materials involved next-generation optoelectronic devices.

Funding. National Natural Science Foundation of China (Grant No. 11804157).

Acknowledgments. The computational resources generously provided by High Perfor- mance Computing Center of Nanjing Tech University are greatly appreciated.

Disclosures. The authors declare no conflicts of interest.

Data availability. Data underlying the results presented in this paper are not publicly available at this time but may be obtained from the authors upon reasonable request.

Supplemental document. See Supplement 1 for supporting content.

References

1. K. S. Novoselov, A. K. Geim, S. V. Morozov, D. Jiang, Y. Zhang, S. V. Dubonos, I. V. Grigorieva, and A. A. Firsov, "Electric field effect in atomically thin carbon films," Science **306**(5696), 666–669 (2004).
2. K. Kim, J. Y. Choi, T. Kim, S. H. Cho, and H. J. Chung, "A role for graphene in silicon-based semiconductor devices," Nature **479**(7373), 338–344 (2011).
3. C. H. Liu, Y. C. Chang, T. B. Norris, and Z. Zhong, "Graphene photodetectors with ultra-broadband and high responsivity at room temperature," Nat. Nanotechnol. **9**(4), 273–278 (2014).
4. S. V. Morozov, K. S. Novoselov, M. I. Katsnelson, F. Schedin, D. C. Elias, J. A. Jaszczak, and A. K. Geim, "Giant intrinsic carrier mobilities in graphene and its bilayer," Phys. Rev. Lett. **100**(1), 016602 (2008).
5. M. Liu, X. Yin, E. Ulin Avila, B. Geng, T. Zentgraf, L. Ju, F. Wang, and X. Zhang, "A graphene-based broadband optical modulator," Nature **474**(7349), 64–67 (2011).
6. M. Liu, X. Yin, and X. Zhang, "Double-layer graphene optical modulator," Nano Lett. **12**(3), 1482–1485 (2012).
7. R. Hao, J. Jin, X. Wei, X. Jin, X. Zhang, and E.-p. Li, "Recent developments in graphene-based optical modulators," Front. Optoelectron. **7**(3), 277–292 (2014).
8. W. Du, R. Hao, and E. P. Li, "The study of few-layer graphene based mach zehnder modulator," Opt. Commun. **323**, 49–53 (2014).
9. H. Karimkhani and H. Vahed, "Hybrid broadband optical modulator based on multi-layer graphene structure and silver nano-ribbons," Opt. Quantum Electron. **52**(5), 229 (2020).
10. Z. Cheng, X. Zhu, M. Galili, L. H. Frandsen, H. Hu, S. Xiao, J. Dong, Y. Ding, L. Oxenløwe, and X. Zhang, "Double-layer graphene on photonic crystal waveguide electro-absorption modulator with 12 ghz bandwidth," Nanophotonics **9**(8), 2377–2385 (2019).
11. J. Wang, J. S. Wang, and Z. Ruan, "Graphene-coated double d-type low loss optical fiber modulator," Opt. Express **29**(2), 2025–2036 (2021).
12. A. N. Grigorenko, M. Polini, and K. S. Novoselov, "Graphene plasmonics," Nat. Photonics **6**(11), 749–758 (2012).
13. H. Li, C. Ji, Y. Ren, J. Hu, M. Qin, and L. Wang, "Investigation of multiband plasmonic metamaterial perfect absorbers based on graphene ribbons by the phase-coupled method," Carbon **141**, 481–487 (2019).

Optics EXPRESS

14. J. P. Liu, X. Zhai, F. Xie, L. L. Wang, S. X. Xia, H. J. Li, X. Luo, and X. J. Shang, "Analytical model of mid-infrared surface plasmon modes in a cylindrical long-range waveguide with double-layer graphene," J. Lightwave Technol. **35**(10), 1971–1979 (2017).
15. H. Li, Y. Zhang, H. Xiao, M. Qin, and L. Wang, "Investigation of acoustic plasmons in vertically stacked metal/dielectric/graphene heterostructures for multiband coherent perfect absorption," Opt. Express **28**(25), 37577–37589 (2020).
16. M. L. Brongersma, *Surface Plasmon Nanophotonics* (Springer Verlag, 2006).
17. S. A. Maier, *Plasmonics: Fundamentals and Applications* (Springer, 2007).
18. W. L. Barnes, A. Dereux, and T. W. Ebbesen, "Surface plasmon subwavelength optics," Nature **424**(6950), 824–830 (2003).
19. Y. Wang, T. Li, L. Wang, H. He, L. Li, Q. Wang, and S. Zhu, "Plasmonic switch based on composite interference in metallic strip waveguides," Laser Photonics Rev. **8**(4), L47–L51 (2014).
20. A. V. Zayats, I. I. Smolyaninov, and A. A. Maradudin, "Nano-optics of surface plasmon polaritons," Phys. Rep. **408**(3-4), 131–314 (2005).
21. D. Ansell, I. P. Radko, Z. Han, F. J. Rodriguez, S. I. Bozhevolnyi, and A. N. Grigorenko, "Hybrid graphene plasmonic waveguide modulators," Nat. Commun. **6**(1), 8846 (2015).
22. Y. Wang, T. Li, and S. Zhu, "Graphene-based plasmonic modulator on a groove-structured metasurface," Opt. Lett. **42**(12), 2247–2250 (2017).
23. S. Qu, C. Ma, and H. Liu, "Tunable graphene-based hybrid plasmonic modulators for subwavelength confinement," Sci. Rep. **7**(1), 5190 (2017).
24. B. Wang, S. Blaize, J. Seok, S. Kim, H. Yang, and R. Salas-Montiel, "Plasmonic-based subwavelength graphene-on-hbn modulator on silicon photonics," IEEE J. Sel. Top. Quantum Electron. **25**(3), 1–6 (2019).
25. C. Zhang, L. Tu, L. Liu, P. Zhan, C. Sun, and Z. Wang, "An electrically tunable plasmonic optical modulator with high modulation depth based on graphene-wrapped silver nanowire," J. Opt. **18**(12), 125007 (2016).
26. Y. Kim and M. S. Kwon, "Mid-infrared subwavelength modulator based on grating-assisted coupling of a hybrid plasmonic waveguide mode to a graphene plasmon," Nanoscale **9**(44), 17429–17438 (2017).
27. Z. Ma, M. H. Tahersima, S. Khan, and V. J. Sorger, "Two-dimensional material-based mode confinement engineering in electro-optic modulators," IEEE J. Sel. Top. Quantum Electron. **23**(1), 81–88 (2017).
28. B. Huang, W. Lu, Z. Liu, and S. Gao, "Low-energy high-speed plasmonic enhanced modulator using graphene," Opt. Express **26**(6), 7358–7367 (2018).
29. R. Hao, Z. Ye, X. Peng, Y. Gu, J. Jiao, H. Zhu, W. Sha, and E. Li, "Highly efficient graphene-based optical modulator with edge plasmonic effect," IEEE Photonics J. **10**(3), 1–7 (2018).
30. F. Sun, L. Xia, C. Nie, C. Qiu, L. Tang, J. Shen, T. Sun, L. Yu, P. Wu, and S. Yin, "An all-optical modulator based on a graphene-plasmonic slot waveguide at 1550 nm," Appl. Phys. Express **12**(4), 042009 (2019).
31. Ren Tangxuan and Chen Lin, "Slow light enabled high-modulation-depth graphene modulator with plasmonic metasurfaces," Opt. Lett. **44**(22), 5446–5449 (2019).
32. Y. Huang, Y. Fang, Z. Zhang, Z. Ling, and M. Sun, "Nanowire-supported plasmonic waveguide for remote excitation of surface-enhanced raman scattering," Light: Sci. Appl. **3**(8), e199 (2014).
33. H. Wei, S. Zhang, X. Tian, and H. Xu, "Highly tunable propagating surface plasmons on supported silver nanowires," Proc. Natl. Acad. Sci. U. S. A. **110**(12), 4494–4499 (2013).
34. R. F. Oulton, V. J. Sorger, T. Zentgraf, R. M. Ma, C. Gladden, L. Dai, G. Bartal, and X. Zhang, "Plasmon lasers at deep subwavelength scale," Nature **461**(7264), 629–632 (2009).
35. L. Yang, T. Hu, A. Shen, C. Pei, B. Yang, T. Dai, H. Yu, Y. Li, X. Jiang, and J. Yang, "Ultracompact optical modulator based on graphene-silica metamaterial," Opt. Lett. **39**(7), 1909–1912 (2014).
36. M. S. Kwon, "Discussion of the epsilon-near-zero effect of graphene in a horizontal slot waveguide," IEEE Photonics J. **6**(3), 1–9 (2014).
37. J. S. Shin, J. S. Kim, and J. T. Kim, "Graphene-based hybrid plasmonic modulator," J. Opt. **17**(12), 125801 (2015).
38. B. Wang, X. Zhang, K. P. Loh, and J. Teng, "Tunable broadband transmission and phase modulation of light through graphene multilayers," J. Appl. Phys. **115**(21), 213102 (2014).
39. P. B. Johnson and R. W. Christy, "Optical constants of the noble metals," Phys. Rev. B **6**(12), 4370–4379 (1972).
40. B. B. Wang, S. Blaize, S. Kim, H. J. Yang, and R. Salas-Montiel, "In-plane electric field confinement engineering in graphene-based hybrid plasmonic waveguides," Appl. Opt. **58**(27), 7503–7509 (2019).
41. L. A. Falkovsky, "Optical properties of graphene," J. Phys. Conf. Ser. **129**, 012004 (2008).
42. V. P. Gusynin, S. G. Sharapov, and J. P. Carbotte, "Unusual microwave response of dirac quasiparticles in graphene," Phys. Rev. Lett. **96**(25), 256802 (2006).
43. V. Sorianello, M. Midrio, and M. Romagnoli, "Design optimization of single and double layer graphene phase modulators in soi," Opt. Express **23**(5), 6478–6490 (2015).
44. M. K. Shah, S. W. Ye, X. H. Zou, F. Yuan, A. Jha, Z. Y. Li, R. G. Lu, and Y. Liu, "Graphene-assisted electroabsorption optical modulator using d-microfiber," IEEE J. Sel. Top. Quantum Electron. **23**(1), 89–93 (2017).
45. Y. Wang, J. Yu, Y. F. Mao, J. Chen, and J. Zhu, "Stable, high-performance sodium-based plasmonic devices in the near infrared," Nature **581**(7809), 401–405 (2020).